Computational Condensed Matter 3 (2015) 41–45

Contents lists available at ScienceDirect

Computational Condensed Matter

journal homepage: http://ees.elsevier.com/cocom/default.asp

Regular article

Ab initio study of the linear and nonlinear optical properties of hexagonal CdSe

C.B. Huang, Z.Y. Wang, H.X. Wu*, Y.B. Ni, R.C. Xiao, M. Qi

Anhui Provincial Key Laboratory of Photonic Devices and Materials, Anhui Institute of Optics and Fine Mechanics, Chinese Academy of Sciences, Hefei 230031, China

ARTICLE INFO

Article history:
Received 22 October 2014
Received in revised form
20 January 2015
Accepted 11 February 2015
Available online 12 February 2015

Keywords:
CdSe
Density functional theory
GW approximation
Optical response

ABSTRACT

We present an ab initio theoretical study of the electronic, linear and nonlinear optical properties of CdSe using a pseudopotential plane-wave method. Since local density approximation (LDA) underestimates its band gap, we used the GW approximation method to calculate its quasiparticle band structure and obtain a band gap 1.67 eV in agreement with experimental value. The GW corrected gap was used as scissor shift to calculate the linear and nonlinear optical properties. Our calculations show that the optical absorption edge is located around 1.7 eV. The intraband and interband contributions to the imaginary part of second-order nonlinear optical susceptibility $\chi^{(2)}_{333}(2\omega, \omega, \omega)$ are presented over a broad energy range. The calculated result for $\left|\chi^{(2)}_{333}(0)\right|$ (at zero frequency limitation) is 74 pm/V, which is close to the experimental value 72 pm/V.

1. Introduction

A great deal of interest has been focused on the II-VI semiconductor compounds such as crystalline CdSe. This interest arises from its potential for many important applications, such as X- and γ-ray detectors, light-amplifiers and laser, as well as nonlinear optical devices [1,2]. At normal pressure, it crystallizes in hexagonal close packed wurtzite structure, which belongs to space group $P6_3mc$. Some experiments were performed to explore its growth technology and characterize its performance [3,4]. There have been several experimental studies of dielectric function [5-7], phonon spectrum [8] and photoelectron spectroscopy [9] of this material, as well as pressure-induced structural phase transitions [10,11]. The first principles were also used to investigate the electrical, structural and elastic properties of wurtzite-type CdSe under pressure [12-15]. Moreover, to overcome the well-known shortcomings of the local density approximation (LDA) or generalized gradient approximations (GGA), especially for the CdSe compound with open-shell 4d valence electrons, D. Vogel et al. [16] calculated the band structures of hexagonal CdSe using self-interaction corrected pseudopotentials. However, little theoretical research has been centered on its linear and nonlinear optical response properties. Thus, it would be meaningful to have a comprehensive analysis of the linear and nonlinear optical properties of hexagonal CdSe from first principles. Since first principle calculations have been successfully used to obtain different properties of bulk semiconductors, such as structural, electronic, linear and nonlinear optical properties [17-22], we presented the first-principles calculation of linear and nonlinear optical properties of hexagonal CdSe using density functional theory (DFT) within the random-phase approximation (RPA) [19] in this work. The GW approximation [23] was used to correct the band gap calculated by generalized gradient approximation (GGA). Then the corrected gap was used as scissor shift to calculate the linear and nonlinear optical properties. This paper is organized in the following way. In Section 2, we give details of our calculations. The electronic ground state properties, optical properties are presented and discussed in Section 3. In Section 4, we summarize our conclusions.

2. Computational details

In this work, calculations were carried out by means of ABINIT code [24]. The ground-state properties were calculated using density functional theory (DFT) method for providing input files for the subsequent excited state computations. The exchange-correlation energy of electrons was evaluated in the generalized gradient approximations (GGA) within the Perdew-Burke-Ernzerhof scheme [25]. An effective ionic potential was

* Corresponding author.
E-mail address: hxwu@ircrystal.com (H.X. Wu).

http://dx.doi.org/10.1016/j.cocom.2015.02.002

approximated by Troullier–Martins type norm-conserving pseudopotentials (NCPPs) [26] and the valence electrons included 4s- and 4p-electrons of Se and 4d- and 5s-electrons of Cd. The electronic wave functions were expanded in terms of a discrete plane-wave basis set with an energy cutoff of ecut = 44Ha. Integration over the Brillouin zone was performed using the Monkhorst and Pack grids [27] with a regular 7 × 7 × 4 mesh. The convergence studies with respect to both ecut and k-points showed that the total energy was converged within 0.0001Ha in these set of both k-points and ecut. To reach equilibrium energy and relative equilibrium volume of CdSe, the Broyden Fletcher Goldfarb Shanno (BFGS) algorithm [28] was used to minimize the total energy and internal forces. After geometry optimizations, the relaxed structures were chosen as input parameters for the following computations.

We first obtained the band structure of CdSe using DFT within the GGA. The result showed that it had a direct band gap with the calculated value of 0.63 eV. As we know, the DFT with the exchange-correlation energy of LDA or GGA could not give the quasi-particle energies correctly and failed to describe optical response [29]. In order to take into account the self-energy effects correctly, we employed a rigorous formulation of the quasiparticle properties in the context of the one-particle Green's function approach [30]. The eigenvalue and eigenfunction of a quasiparticle in a crystal are described Dyson equation

$$\widehat{H}_0\left(\vec{r}\right)\varphi_i\left(\vec{r}\right) + \int \Sigma\left(\vec{r},\ \vec{r}^{\,\prime};\omega_i\right)\varphi_i\left(\vec{r}^{\,\prime}\right)d^3\vec{r}^{\,\prime} = \varepsilon_i\varphi_i\left(\vec{r}\right), \qquad (1)$$

where $\widehat{H}_0(\vec{r})$ includes the kinetic-energy operator and Hartree potential of the electrons, as well as external potential from ions. The nonlocal and frequency-dependent function $\Sigma(\vec{r},\ \vec{r}\ ;\omega_i)$ is the non-Hermitian self-energy operator, which contains all many-body exchange-correlation effects. It can be obtained by solving Hedin equation with one-shot GW or G_0W_0 method [31]. The G_0 was obtained from independent-particle propagator of the Kohn-Sham (KS) Hamiltonian and the screened interaction W_0 (screening file) is approximated with the RPA calculated with KS energies and wave functions. It is noted that the screened interaction is evaluated by numerical integration model which require large CPU time but could give the most accurate results. After getting ground state density, calculation was carried out to obtain KS eigenfunctions and band structure (KSS file) which stored 240 bands. Specifically, the convergence studies were performed respecting to the number of plane waves in screening calculation and the number of bands in screening in self-energy calculations, as well as the k-point mesh. The results showed that the total energy was converged within 0.0001Ha with nband = 200 and ecuteps = 7 in screening calculation, nband = 220 in self-energy calculation and a regular 14 × 14 × 8 mesh.

3. Result and discussion

3.1. Structural and electrical properties

The original cell of CdSe with hexagonal structure is displayed in Fig. 1. It belongs to point group 6 mm and has four atoms in a primitive cell. Instead of using exchange-correlation energy of local density approximation (LDA), the semilocal density approximation, generalized gradient approximations (GGA), was adopted for the inhomogeneous semiconductor system. The structural optimizations were carried out by two steps: first to optimize the ionic positions without cell shape and size optimization, then start the cell shape and size optimization from the cell with relaxed ionic positions. Calculations were carried out using the lattice constant a = b = 4.299 Å, c = 7.011 Å [32] and the optimized results are

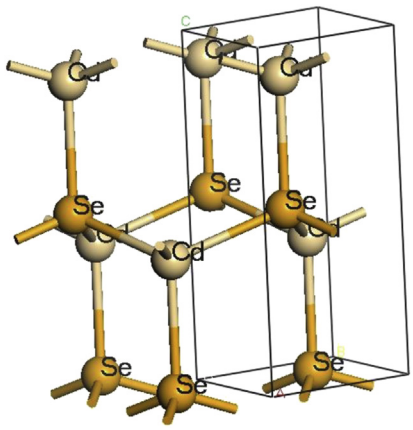

Fig. 1. Crystal structure of hexagonal CdSe. Yellow and off-white spheres represent Se and Cd atoms, respectively.

a = b = 4.347 Å, c = 7.029 Å. The lattice parameters of CdSe obtained from the structure optimization are presented in Table 1 along with other calculations and experimental data reported in the literature. Our calculations estimate the equilibrium values with the maximal error of only 1.1% with respect to experimental values. It is largely sufficient to allow the further study of electric, optical properties for CdSe.

The band structure of CdSe along the lines of high symmetry points in the Brillouin zone are showed in Fig. 2. Both valence band maximum and conduction band minimum are located at Γ point, so CdSe has a direct band gap with the calculated value of 0.63 eV. The result is severe underestimation compared with the experiment value (1.74 and 1.8 eV) [16,33]. The band gaps of hexagonal CdSe obtained from this work are presented in Table 1 along with other calculations and experimental data reported in the literature. These underestimations are due to the shortcomings of approximate exchange–correlation function, such as self-interaction of the LDA or GGA potential and the lack of a discontinuity in the exchange potential. To obtained exact exchange potential, D. Vogel et al. [16] have used self-interaction corrected (SIC) pseudopotentials method and improved the band gap of hexagonal CdSe to 1.27 eV. In this paper, we modify the band structure of CdSe for Γ point with 18 and 19 bands using GW approximation. Our calculations show that GW corrections widened the energy gaps. The calculated energy gap is 1.67 eV at Γ point. This is substantially larger than the GGA value of 0.63 eV and closer to the experimental value of 1.74 eV and 1.80 eV. The gap due to the GW correction can be used as a scissor shift to calculate the linear and nonlinear optical properties in next steps.

Table 1
Crystal structure data and band gap of hexagonal CdSe compared with both experimental and theoretical data.

	Exp.	Theo.	This work
Lattice parameters	a = b = 4.299 Å[e] c = 7.011 Å[e]	a = b = 4.200 Å[d] c = 6.804 Å[d] a = b = 4.29 Å[c] c = 7.02 Å[c]	a = b = 4.347 Å c = 7.029 Å
Band gap E_g	1.7 eV[a] 1.74 eV[b] 1.8 eV[c]	0.51 (LDA)[c] 1.27 (SIC)[c]	0.63 (GGA) 1.67 (GW)

[a] Ref. [4].
[b] Ref. [33].
[c] Ref. [16].
[d] Ref. [13].
[e] Ref. [32].

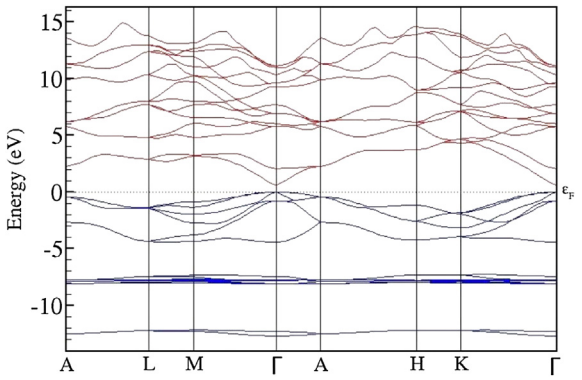

Fig. 2. Calculated band structure for hexagonal CdSe single crystal.

3.2. Optical response

In a nonlinear media, the second-order nonlinear optical phenomena can be described by a Taylor series expansion of the polarization $\vec{P}(t)$ at time t in terms of electrical field $\vec{E}(t)$:

$$\vec{P} = \varepsilon_0 \chi_{ij}^{(1)} \cdot \vec{E} + \varepsilon_0 \chi_{ijk}^{(2)} : \vec{E}\vec{E} + \cdots, \quad (2)$$

where the second-rank tensor $\chi_{ij}^{(1)}$ is linear dielectric susceptibility related to the linear dielectric function ε_{ij} and the third-rank tensor $\chi_{ijk}^{(2)}$ is second-order nonlinear optical susceptibility related to second-order nonlinear optical coefficient d_{ijk}. These tensor components are determined by the permutation of the Cartesian components i, j, k. Since the CdSe crystal belongs to point group 6 mm, there are two independent component of linear dielectric susceptibility, 11 and 33, and three independent component of second-order nonlinear optical susceptibility, 333, 311 and 113, respectively. The optical responses are influenced by electron state transitions, electron–hole interactions (excition effects), and phonon effects. In fact, the electron state transitions are the biggest contributor, especially in the intrinsic absorption region. They could be described by random-phase approximation (RPA) within the frame of DFT. The expressions in Eq. (46), Eq. (49) and Eq. (50) in Ref. [19] give linear and second-order nonlinear susceptibility within the RPA. Where, the position matrix elements r_{mn} are determined by response wavefunction which is computed by density functional perturbation theory (DFPT) [18]. To get the optical spectrum and make a realistic comparison with experiments, both a large number of bands (90) and a dense sampling of k-points ($24 \times 24 \times 14$) are set in this work. What is more, the band gap of CdSe is scissor corrected by 1.04 eV which is the difference between the GGA calculated value (0.63 eV) and GW corrected band gap (1.67 eV).

3.2.1. Linear optical response

Linear optical properties of materials, refractive index and extinction coefficient, can be deduced from complex dielectric function $\varepsilon(\omega)$ given by $\varepsilon(\omega) = \varepsilon_1 + i\varepsilon_2$. The imaginary part of the dielectric function can be obtained from Random-phase approximation (RPA) and the real part of the spectrum is related by the Kramers–Kronig relation to the imaginary part. According to Eq. (46) in Ref. [19], for semiconductor only the interband transitions contribute to the imaginary part of the dielectric. It is reasonable for wide band-gap semiconductor CdSe to neglect the indirect intraband transitions which is connected to free carrier absorption involving scattering of phonons. The calculated and experimental imaginary parts of the frequency dependent linear dielectric function of ε_{11} and ε_{33} are shown in Fig. 3(a) and (b) respectively. The calculated spectra are zero below 1.7 eV (the direct band gap) and decrease beyond 7 eV. Several peaks in the spectra correspond to electronic transitions from the valence band to the conduction band. The comparing experimental results [6,7] are also presented in Fig. 3(a) and (b). The dash line and dot line corresponding to T=300 K and T=210 K respectively with the range from 0 to 5 eV. As seen from Fig. 3, the calculated major peaks are located at 4.4 eV, 5 eV, and 7 eV in ε_{11} spectra and 4.6 eV and 6.9 eV in ε_{33} spectra which are similar to the experimental ones. However, their magnitudes have deviations from the experimental values. The peak of 4.4 eV in ε_2^{11} spectra is about 7 in our calculation, while the corresponding experimental value is about 7.5 at 4.2 eV. The peak of 4.7 eV in ε_2^{33} spectra is about 9.5 in our calculation, while the corresponding experimental value is about 10.6 at 4.6 eV. It is noted that the density functional theory adopts Born-Oppenheimer (adiabatic) approximation and independent particle approximation. Since the presences of excition effects are not included in this theory, the different between experimental and theoretical is predictable from 2 to 5 eV. The Bethe-Salpeter theory may improve the results but require huge computation.

From the Kramers–Kronig relation, we obtain the real part of the dielectric function ε_1 (the component of 11 and 33). The calculated spectra are shown in Fig. 4. The static dielectric constant $\varepsilon_1(0)$ is given by the low energy limit of $\varepsilon_1(\omega)$. Because of the adiabatic approximation, the phonon perturbations are not included in the calculations. The zero frequency limitation of $\varepsilon_1^{11}(0)$ and $\varepsilon_1^{33}(0)$ in our calculations are 6.71 and 6.70 which have little deviation from the experimental value 6.59 and 6.62 [14,15]. Noted that the static dielectric constant depends strongly on the band gap (electric part) [34]. This can be explained by the expression of Penn model, $\varepsilon(0) \approx 1 + (\hbar\omega/2\pi E_g)^2$. It is clear that $\varepsilon(0)$ is inversely proportional to E_g. Therefore, the GW corrected band gap plays a key role for calculating static dielectric constant. The calculated refractive indexes are displayed in Fig. 5. Since nonlinear frequency conversion is one of its applications, some experiments [35,36] have been performed to measure its refractive indexes in the infrared region. Unfortunately, our calculated results of refractive indexes are larger than the experimental value, while the birefringence is smaller in the near infrared zone. The results agree

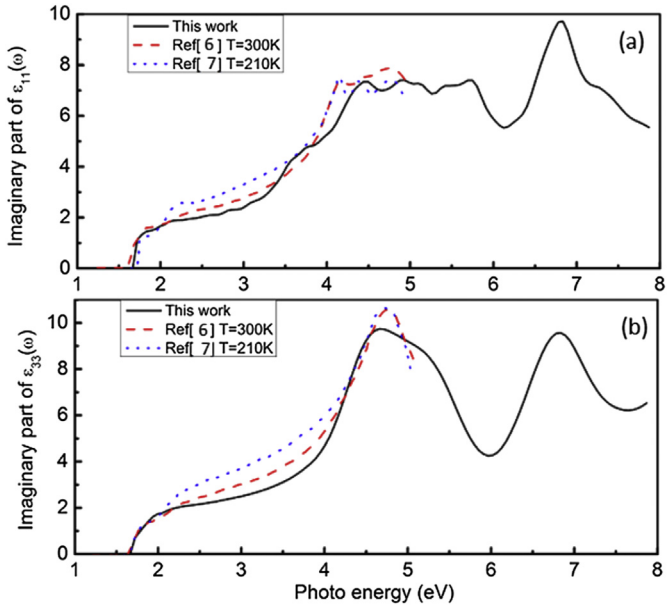

Fig. 3. The imaginary parts of optical dielectric function (a) E⊥c and (b) E∥c of hexagonal CdSe crystal. For comparison, the experimental data obtained at 210 K and 300 K are also shown by the dashed lines.

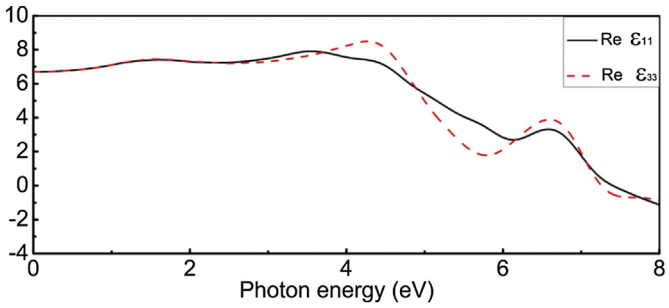

Fig. 4. The real part of optical dielectric function of hexagonal CdSe crystal.

with other theoretical work for semiconductor [37,38] and the deviations derive from the absence of electron–hole interaction and electron–phonon interaction in the frame of density functional theory. As we known, so far there is no fruitful theory for predicting the refractive indexes in the infrared region due to the complexity of phonon perturbations. According to Fig. 3, the average absorption edge is located at 1.7 eV, which is in good agreement with the experimental values. It is noted that the value of absorption edge depends strongly on the shifted corrected band gap.

3.3. Nonlinear optical response

Nonlinear optics has important applications in many technical areas such as optoelectronics, laser science, and optical signal processing. The second-order nonlinear optical susceptibility plays an important role in nonlinear optical phenomena. In general, the static second harmonic generation (SHG) susceptibility could be obtained from experiment. However, the experimental measurements could not give the frequency-dependent second-order nonlinear optical susceptibility. In this section, we will present the results for the different contributions to the imaginary part of second-order nonlinear optical susceptibility and static SHG susceptibility.

Since we consider the frequency-dependent $\chi^{(2)}_{ijk}(2\omega,\omega,\ \omega)$ function, the Kleninman symmetry is not applied in this calculation. The three independent $\chi^{(2)}_{ijk}(2\omega,\omega,\ \omega)$ component, 113, 333, and 311 are calculated in this work. In order to understand the different contributions to second-order susceptibility, we take the $\chi^{(2)}_{333}$ as an example. Fig. 6 demonstrates the magnitudes of the interband and intraband contributions to the imaginary part of second-order susceptibility $\chi^{(2)}_{333}(2\omega,\omega,\ \omega)$, from which the real part can be obtained by the Kramers–Kronig relations. As can be seen the total second-order susceptibility is vanished at zero energy. The 2ω terms start contributing at energy about $1/2E_g$ and the 1ωfor the energy values above E_g. In the low energy region (<5.5 eV), the second-order susceptibility optical spectra are

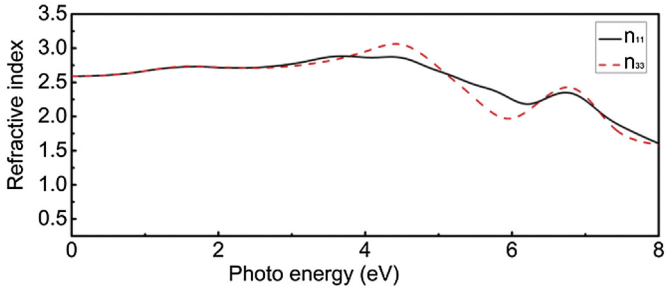

Fig. 5. The refractive index of hexagonal CdSe crystal.

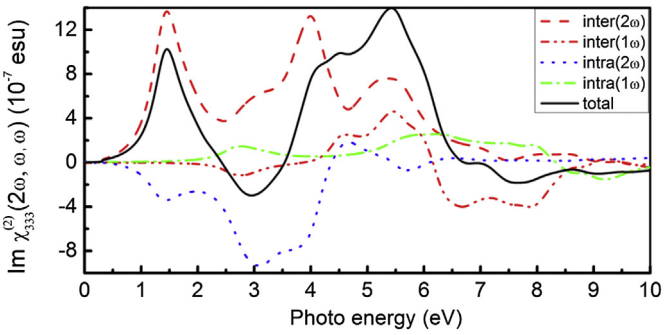

Fig. 6. Calculated total $\mathrm{Im}\chi_{333}{}^{(2)}(2\omega,\omega,\omega)$ spectra along with the intra-(2ω)/(1ω) and inter-(2ω)/(1ω) band contributions for hexagonal CdSe.

dominated by the 2ω contributions. Beyond 6 eV the major contributions come from the 1ω terms. Unlike the linear optical spectra, the features in the second-order susceptibility are very difficult to identify from the band structure because of the complicated resonance of the 2ω and 1ω terms.

To our knowledge, the lack of experimental data prevents any conclusive comparison with experiment over a large energy range. Therefore, we focus on the magnitude of second-order susceptibility, rather than identifying the different resonances leading to various features in the NLO spectra. In Fig. 7, we plot the modulus value of the complex second-order susceptibility $\chi^{(2)}_{333}$, $\chi^{(2)}_{311}$ and $\chi^{(2)}_{113}$. As a whole, the spectra increase from 0 eV and decrease beyond 7 eV. The static dielectric constant is given by the zero frequency limitation of second-order susceptibility $\chi^{(2)}_{333}(2\omega,\ \omega,\ \omega)$. The magnitude of $|\chi^{(2)}_{333}(0)|$(at zero frequency limiting), corresponding to the value $2d_{33}$ (second-order nonlinear optical coefficients), is 74 pm/V which is very close to the experiment value (72 pm/v) [39]. The value of $|\chi^{(2)}_{311}(0)|$, corresponding to the $2d_{33}$, is 63 pm/V which is larger than the experiment value (36 pm/V) [37]. The calculated value of $|\chi^{(2)}_{113}(0)\ |$, corresponding to the value of $2d_{15}$, is 11 pm/V and is small below 2 eV.

4. Conclusion

In the present work, the electrical, linear and nonlinear properties of CdSe have been investigated from first principles. It is found that the results of implemented structural optimization by the GGA and the experiments agree with each other well. Calculated results for band structure show that the CdSe has a direct band gap with the calculated value to be 0.63 eV. The GW corrected band gap is 1.67 eV which is close to experimental value (1.74 eV).

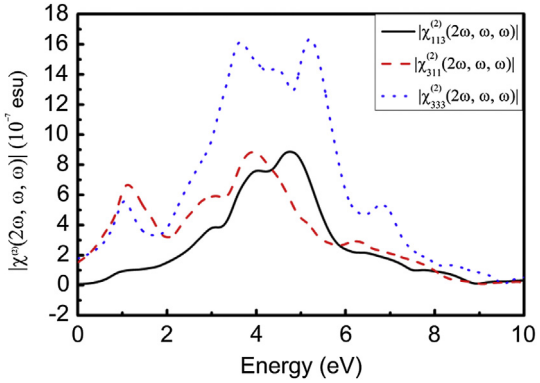

Fig. 7. Absolute value of the second-order nonlinear susceptibility for hexagonal CdSe.

The calculated absorption spectrum indicate that CdSe are transmitting for frequencies <1.7 eV. The calculated results for frequency dependent dielectric function demonstrate several main peaks, corresponding to electronic transitions from the valence band to the conduction band, beyond the band gap energy. The location and magnitude of these peaks are close to the experimental data. We deduce that the deviations between theoretical and experimental value derive from the thermal effects and excited effects. The Bethe-Salpeter theory which includes excited effects may improve the results very well but require huge computation. The intra- and inter-band contributions to the imaginary part of $\chi^{(2)}_{333}(2\omega, \omega, \omega)$ are presented over a broad energy range. Our calculated second-order susceptibility, $|\chi^{(2)}_{333}(0)|$ (at zero frequency limiting), is closed to the experimental value 72 pm/V.

Acknowledgments

This work made use of Center for Computational Science, CASHIPS.

References

[1] K.L. Vodopyanov, Mid-infrared optical parametric generator with, J. Opt. Soc. Am. B 16 (1999) 1579–1586.
[2] P. Yu Gnatenko, P.M. Bukivskij, I.O. Faryna, et al., Photoluminescence of high optical quality CdSe thinfilms deposited by close-spaced vacuum sublimation, J. Lumin 146 (2014) 174–177.
[3] O.D. Melo, E.M. Larramendi, I.M. Bacho, et al., Growth of CdSe and CdTe crystals shaped by thick alumina membranes, J. Cryst. Growth 311 (2008) 26–31.
[4] T.X. Zeng, B.J. Zhao, S.F. Zhu, et al., Optimizing the growth procedures for CdSe crystal by thermal analysis techniques, J. Cryst. Growth 316 (2011) 15–19.
[5] S. Adachi, Model dielectric function of hexagonal CaSe, J. Appl. Phys. 68 (1990) 1192–1199.
[6] S.S. Ninomiya, S.D. Adachi, Optical properties of cubic and hexagonal CdSe, J. Appl. Phys. 78 (1995) 4681–4688.
[7] C. Janowitz, O. Giinther, G. Jungk, et al., Dielectric function and critical points of cubic and hexagonal CdSe, Phys. Rev. B 50 (1994) 2181–2187.
[8] A.K. Arora, A.K. Ramdas, Resonance Raman scattering from defects in CdSe, Phys. Rev. B 35 (1987) 4345–4350.
[9] K.O. Magnusson, U.O. Karlsson, D. Straub, et al., Angle-resolved inverse photoelectron spectroscopy studies of CdTe(110), CdS(1120), and CdSe(1120), Phys. Rev. B 36 (1987) 6566–6573.
[10] H. Sowa, The high-pressure behaviour of CdSe up to 3 GPa and the orientation relations between its wurtzite- and NaCl-type modifications, Solid State Sci. 7 (2005) 1384–1389.
[11] C.Y. He, C.X. Gao, Y.Z. Ma, et al., Electrical property and phase transition of CdSe under high pressure, J. Phys. Chem. Solids 69 (2008) 2227–2229.
[12] M. Co˚te ', O. Zakharov, A. Rubio, et al., Ab initio calculations of the pressure-induced structural phase transitions for four II-VI compounds, Phys. Rev. B 55 (1997) 13025–13031.
[13] O. Zakharov, A. Rubio, M.L. Cohen, et al., Calculated structural and electronic properties of Cdse under pressure, Phys. Rev. B 51 (1995) 4926–4930.
[14] E. Deligoz, K. Colakoglu, Y. Ciftci, et al., Elastic, electronic, and lattice dynamical properties of CdS, CdSe, and CdTe, Phys. B 373 (2006) 124–130.
[15] J.W. Yang, H.J. Hou, A first-principles study on the structural and elastic properties and the equation of state of wurtzite-type cadmium selenide under pressure, High Press. Res. 32 (2012) 376–384.
[16] D. Vogel, P. Kriiger, J. Pollmann, et al., Ab initio electronic-structure calculations for II-VI semiconductors using self-interaction-corrected pseudopotentials, Phys. Rev. B 54 (1995) R14314–R14319.
[17] M.C. Payne, M.P. Teter, D.C. Ailan, et al., Iterative minimization techniques for ab initio total-energy calculations: molecular dynamics and conjugate gradients, Rev. Mod. Phys. 64 (1992) 1045–1097.
[18] S. Baroni, S.D. Gironcoli, A. Dal Corso, et al., Phonons and related crystal properties from density-functional perturbation theory, Rev. Mod. Phys. 73 (2001) 515–562.
[19] S. Sharma, C. Ambrosch-Draxl, Second-harmonic optical response from first principles, Phys. Scr. 109 (2004) 128–134.
[20] J.L.P. Hughes, J.E. Sipe, Calculation of second-order optical response in semiconductors, Phys. Rev. B 53 (1996) 751–763.
[21] J.L.P. Hughes, Y. Wang, J.E. Sipe, Calculation of linear and second-order optical response in wurtzite GaN and AlN, Phys. Rev. B 55 (1997) 630–640.
[22] J.E. Sipe, A.I. Shkrebtii, Second-order optical response in semiconductors, Phys. Rev. B 61 (2000) 5337–5352.
[23] G. Onida, L. Reining, A. Rubio, et al., Electronic excitations: density-functional versus many-body Green's-function approaches, Rev. Mod. Phys. 74 (2002) 601–659.
[24] X. Gonze, J.-M. Beuken, R. Caracas, F. Detraux, M. Fuchs, G.-M. Rignanese, L. Sindic, M. Verstraete, G. Zerah, F. Jollet, M. Torrent, A. Roy, M. Mikami, Ph. Ghosez, J.-Y. Raty, D.C. Allan, Comput. Mater. Sci. 25 (2002) 478. http://www.abinit.orgs.
[25] J.P. Perdew, S. Burke, M. Ernzerhof, et al., Generalized gradient approximation made simple, Phys. Rev. Let. 77 (1996) 3865–3868.
[26] N. Troullier, J.L. Martins, Efficient pseudopotentials for plane-wave calculations, Phys. Rev. B 43 (1991) 1993–2006.
[27] H.J. Monkhorst, J.D. Pack, Special points for Brillouin-zone integrations, Phys. Rev. B 13 (1976) 5188–5192.
[28] T.H. Fischer, J. Almlof, General methods for geometry and wave function optimization, J. Phys. Chem. 96 (1992) 9768–9774.
[29] A. Seidl, A. GÖrling, Generalized Kohn-Sham schemes and the band-gap problem, Phys. Rev. B 53 (1996) 3764–3774.
[30] Giovanni Onida, Lucia Reining, Angel Rubio, Electronic excitations:density-functional versus many-body Green's-function approaches, Rev. Mod. Phys. 74 (2002) 601–659.
[31] F. Aryasetiawany, O. Gunnarsson, The GW method, Rep. Prog. Phys. 61 (1998) 237–312.
[32] I.D. Olekseyuk, O.V. Parasyuk, O.A. Dzham, et al., The reciprocal CuInS2+2CdSe□CuInSe2+2CdS system. Part I. The quasi-binary CuInS, J. Solid State Chem. 179 (2006) 315–322.
[33] B. Jensen, A. Torabi, Refractive index of hexagonal II-VI compounds CdSe, CdS, and CdSeS, J. Opt. Soc. Am. B 3 (1986) 857–863.
[34] D.R. Penn, Wave-number-dependent dielectric function of semiconductors, Phys. Rev. 128 (1962) 2093.
[35] W.L. Bond, Measurement of the refractive indices of several crystals, J. Appl. Phys. 36 (1965) 1674–1677.
[36] M.P. Lisitsa, L.F. Gudymenko, V.N. Malinko, et al., Dispersion of the refractive indices and birefringence of CdSSe single crystals, Phys. Stat. Solidi 31 (1969) 389–399.
[37] S.N. Rashkeev, S. Limpijumnong, R.L. Lambrecht, et al., Second-harmonic generation and birefringence of some ternary pnictide semiconductors, Phys. Rev. B 59 (1999) 2737.
[38] S.R. Zhang, S.F. Zhu, B.J. Zhao, et al., First-principles study of the elastic, electronic and optical properties of ε-GaSe layered semiconductor, Phys. B 436 (2014) 188–192.
[39] D.A. Roberts, Simplified characterization of uniaxial and biaxial nonlinear optical crystals: a plea for standardization of nomenclature and conventions, J. Quant. Electr. 28 (1992) 2057–2074.